Cospectral budget model describes incipient sediment motion in turbulent flows

Shuolin Li*
Sibley School of Mechanical and Aerospace Engineering, Cornell University, Ithaca, New York, USA and Nicholas School of the Environment, Duke University, Durham, North Carolina, USA

Gabriel Katul
Nicholas School of the Environment and Department of Civil and Environmental Engineering, Duke University, Durham, North Carolina, USA

(Received 17 May 2019; published 24 September 2019)

Relating incipient motion of sediments to properties of turbulent flows continues to draw significant research attention given its relevance to a plethora of applications in ecology, sedimentary geology, geomorphology, and civil engineering. Upon combining several data sources, an empirical diagram between a densimetric Froude number $F_{dc} = U_c/\sqrt{gh\Delta}$ and relative roughness $N = d/h$ was recently reported over some six decades of N, where d is the grain diameter, h is the overlying boundary-layer depth, U_c is the bulk velocity at which sediment motion is initiated, g is the gravitational acceleration, $\Delta = s - 1$, and s is the specific gravity of sediments. This diagram featured three approximate scaling laws of the form $F_{dc} \sim N^{-\alpha}$ with $\alpha = 1/2$ at small N, $\alpha = 1/6$ at intermediate N, and $\alpha = 0$ at large N. The individual α values were piecewisely recovered using a combination of (1) scaling arguments linking bulk to local flow variables above the sediment bed and (2) assumed exponents σ for the turbulent kinetic energy spectrum $E_{tke}(k) \sim k^{-\sigma}$, where k is the wave number or inverse eddy size. To explain the $\alpha = 1/2$, the aforementioned derivation further assumed the presence of an inverse cascade in $E_{tke}(k)$ at large wave number (i.e., $\sigma = 3$). It is shown here that a single $F_{dc} - N$ curve can be derived using a cospectral budget (CSB) model formulated just above the sediment bed. For any k, the proposed CSB model includes two primary mechanisms: (1) a turbulent stress generation formed by the mean velocity gradient and the spectrum of the vertical velocity $E_{ww}(k)$ and (2) a destruction term formed by pressure-velocity interactions. Hence, a departure from prior work is that the proposed CSB model is driven by a multiscaled $E_{ww}(k)$ instead of $E_{tke}(k)$ characterized by a single exponent. Also, the CSB model does not require the presence of an inverse cascade to recover an $\alpha = 1/2$. Last, the CSB approach makes it clear that the scaling parameters linking local to bulk flow variables used in prior determinations of α at various N must be revised to account for bed roughness effects.

DOI: 10.1103/PhysRevFluids.4.093801

I. INTRODUCTION

Incipient motion of grains by turbulent flows over a loose boundary continues to draw research attention in erosion studies, river bank stability, ecosystem sciences, and eolian processes [1–3]. Over the course of some 100 years, such incipient motion has been described using a balance between hydrodynamic forces exerted on particles and a stabilizing force represented by the

*sl3259@cornell.edu

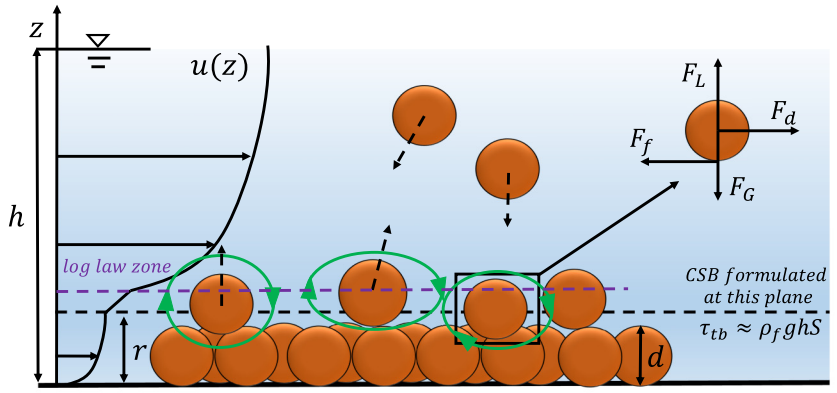

FIG. 1. Sketch of a wide rough channel whose bed is covered by spherical grain particles of uniform diameter d. The grains are entrained into the overlying turbulent flow when the surface shear stress τ_{tb} exceeds a threshold. The green arrow depicts turbulent eddies that have multiple sizes, and the grains are represented by brown circles. The cospectral budget (CSB) model is formulated in the roughness sublayer (black dashed line) above the grains but below the region characterized by a logarithmic mean velocity profile (purple dashed line). The forces acting on an individual particle are defined as follows: F_d is the drag force, F_f is the frictional force, F_G is the gravitational force related to particle weight, and F_L is the lift force.

submerged particle weight as shown in Fig. 1. This force balance has been developed at the single-particle scale [4] but extrapolated in space to account for multiparticle interactions using probabilistic approaches [5]. Extensions to both have also been proposed and used in a number of applications [6–8].

Operationally, incipient motion is described by the *Shields diagram* [9] that empirically relates a dimensionless bed shear stress θ (labeled as the critical Shields number)

$$\theta = \frac{u_*^2}{\Delta g d} \tag{1}$$

to a roughness Reynolds number Re_* [10–12]. It is to be noted that when the shear or friction velocity u_* reaches the critical shear velocity u_{*c} and the sediment particle is about to move, the Shields number becomes the critical Shields number θ_c. Here the roughness Reynolds number is defined as $\mathrm{Re}_* = u_* d/\nu$, where $\Delta = s - 1 > 0$, $s = \rho_p/\rho_f$ is the specific gravity of the particles, ρ_p and ρ_f are the particle and water densities respectively, g is the gravitational acceleration, ν is the kinematic viscosity, $u_* = (\tau_b/\rho_f)^{1/2}$ is the friction velocity, τ_b is the bed shear stress, and d is the grain diameter. Figure 2 repeats such a diagram summarizing a large corpus of experiments. This diagram shows that at low Re_*, θ_c decreases with increasing Re_*, whereas θ_c becomes a constant independent of Re_* for large Re_*. While the limitations of the Shields diagram have been recognized for some time [1,13], the data presentation inspired by the Shields diagram remains popular in numerous fields. Its simplicity and reasonable empirical support [14,15] even in situations that fall well outside the original domain of applicability [16–21] continue to make the θ_c-Re_* representation attractive and a test bed for other detailed models [22]. A case in point is the use of a Shields diagram to reconstruct a number of surface features on Mars [23,24] and Titan [25].

An even more "naive" but preferable approach in large-scale hydrodynamic models is to use a critical bulk velocity U_c formed by a flow rate per unit cross-sectional area instead of the critical shear velocity to scale particle incipient motion. This approach gained attention after Ali and Dey [3,26] reported a remarkable link between a densimetric Froude number $F_{dc} = U_c/\sqrt{\Delta g d}$ and relative roughness $N = d/h$ shown in Fig. 3, where h is the boundary layer depth (or water level in wide channels). The reported relation appears to be valid over six decades of N with F_{dc} exhibiting

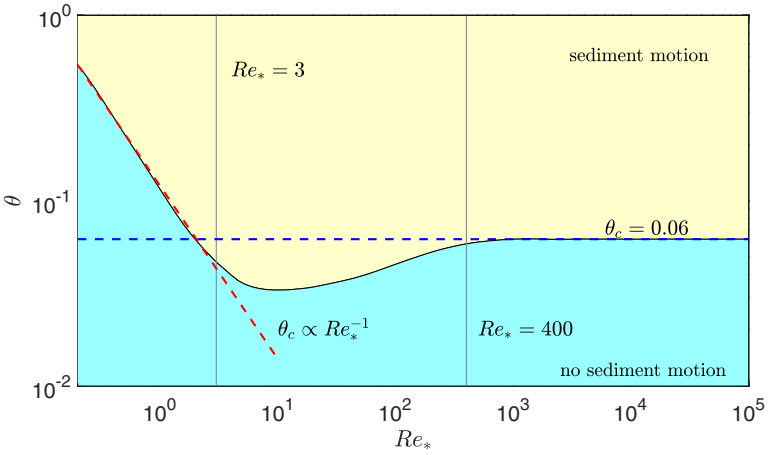

FIG. 2. Modified Shields diagram fitted to the original data of Shields [9], where $\theta_c \approx 0.06$ is independent of Re_* when $\mathrm{Re}_* > 400$ and $\theta_c \propto \mathrm{Re}_*^{-1}$ for $\mathrm{Re}_* < 3$. An intermediate region defined by $\mathrm{Re}_* \in [3, 400]$ exists where $\theta \in [0.02, 0.06]$ varies weakly and nonmonotonically with Re_*.

at least 1.5 decades of variations. Another outcome in Fig. 3 is the presence of three regimes featuring approximate scaling laws of the form $F_{dc} \sim N^{-\alpha}$: $\alpha = 1/2$ for the so-called miniroughness regime $N \in [10^{-6}, 10^{-4}]$, $\alpha = 1/6$ for the small-roughness regime $N \in [10^{-4}, 0.1]$, and $\alpha = 0$ for the large-roughness regime $N \in [0.1, 1]$.

Instead of using separate arguments to explain each α value, it is shown here that a single F_{dc}-N curve can be recovered from a cospectral budget (CSB) model that tracks the effects of all eddies on τ_b. The proposed model is driven by the shape of the vertical velocity spectrum $E_{ww}(k)$ instead of the turbulent kinetic energy spectrum $E_{tke}(k)$. That $E_{ww}(k)$ explains the F_{dc}-N curve is to be expected in vertical momentum transfer studies of wall stress. Moreover, the work here shows that the presence of an inverse cascade is not necessary provided some steepening of the $E_{ww}(k)$ above and beyond its inertial scaling occurs at small scales. However, links between local variables in the roughness sublayer above the bed and bulk variables must be revised to account for roughness effects as

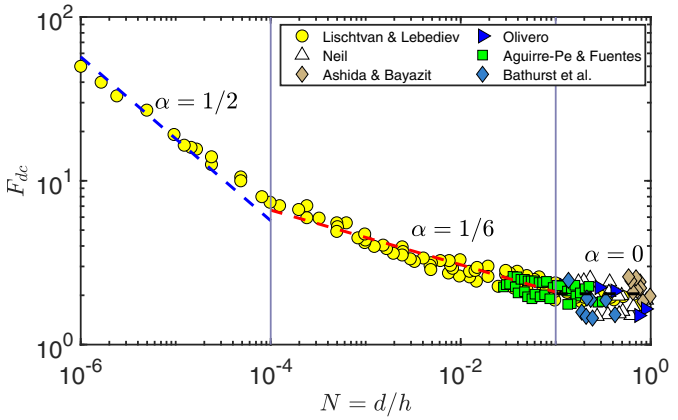

FIG. 3. The F_{dc}-N diagram with data reported in Refs. [3,26] along with the three scaling laws expressed as $F_{dc} \sim N^{-\alpha}$ with $\alpha = 1/2$, $1/6$, and 0 (in dashed lines). The original data sources are described in a number of studies, including Refs. [27–33].

discussed elsewhere [34]. The main theoretical insights offered here are perspectives about the curve featured in Fig. 3, the transition zones between the various roughness scaling regimes, and the links between exponents α and the entire shape of $E_{ww}(k)$ that is characterized by multiple exponents. It also offers a pragmatic approach (i.e., a single expression) to modeling incipient motion within large-scale hydrodynamic models of sediment motion when U_c is to be used.

II. THEORY

A. Review of the analysis by Ali and Dey

The insightful analysis by Ali and Dey [3,26] to explain the three piecewise scaling laws in Fig. 3 is reviewed. At the point of incipient sediment motion (i.e., $U = U_c$) and from the aforementioned definitions, it directly follows that F_{dc} can be linked to θ_c using

$$F_{dc} = \frac{U_c}{\sqrt{\Delta g d}} = \frac{u_*}{\sqrt{\Delta g d}} \frac{U_c}{u_*} = \sqrt{\theta_c} \frac{U_c}{u_*}. \tag{2}$$

When $\mathrm{Re}^* > 400$ (i.e., fully rough flow regime), the Shields diagram in Fig. 2 suggests that θ_c approaches a constant value independent of Re_* and F_{dc} is determined entirely from U_c/u_*. The aforementioned studies [3,26] assumed that the flow is fully rough and θ_c is constant for differing N ranges. It was further assumed that $u_*^2 = v_l U_c$, where v_l is a characteristic turbulent vertical velocity [35], whereas horizontal velocity turbulent excursions scale with U_c. To determine v_l, a phenomenological model was then used given as [3,26,36]

$$v_l \sim \left[\int_{l^{-1}}^{\infty} E_{tke}(k)\, dk \right]^{1/2}, \tag{3}$$

where l is a characteristic length scale of the eddy near the roughness bed assumed proportional to d [3,26]. The $E_{tke}(k)$ is modeled with a single exponent so that $E_{tke}(k) \propto k^{\sigma}$. Based on dimensional analysis alone, Ali and Dey [3,26] argued that $E_{tke}(k)$ must be related to bulk variables (U_c, h) only, and k so that

$$\frac{E_{tke}(k)}{U_c^2 h} = A_e (kh)^{\sigma}. \tag{4}$$

In principle, $E_{tke}(k)$ must be formulated in the same plane (i.e., roughness sublayer) where τ_c is acting (see Fig. 1). This colocation means that the scaling in Eq. (4) may be plausible when local variables in this plane are linked to bulk variables without any roughness modifications. Inclusion of roughness effects may be possible if the similarity constant A_e in Eq. (4) is made to vary with a roughness length that depends on d. However, the work of Ali and Dey was focused on links between σ and α and ignored this revision. Accepting their arguments leading to Eq. (4), substituting Eq. (4) into Eq. (3), and integrating leads to

$$\frac{v_l}{U_c} \sim \left(\frac{d}{h} \right)^{-(1+\sigma)/2}. \tag{5}$$

With this estimate of v_l, the turbulent shear shear stress τ_c can be computed from

$$\tau_c = \rho u_*^2 \sim \rho v_l U_c \sim \rho U_c^2 \left(\frac{d}{h} \right)^{-(1+\sigma)/2}. \tag{6}$$

Inserting Eq. (6) into Eq. (2), the densimetric Froude number can now be derived as [3],

$$F_{dc} \sim \sqrt{\theta_c} \left(\frac{d}{h} \right)^{(1+\sigma)/4} = \sqrt{\theta_c} (N)^{(1+\sigma)/4}; \tag{7}$$

that is, $\alpha = -(1+\sigma)/4$. This completes the sought link between the scaling laws in the F_{dc}-N curve shown in Fig. 3 and exponents describing the decay of $E_{tke}(k)$ with decreasing eddy sizes. The three

scaling regimes in the F_{dc}-N diagram can be piecewise recovered when assuming differing energy transfer mechanisms dominate the $E_{tke}(k)$:

(1) When $\sigma = -5/3$, which is the scaling law expected for the inertial subrange for locally homogeneous and isotropic turbulence, an $\alpha = 1/6$ is recovered.

(2) When $\sigma = -1$, which is the scaling law linked to attached eddies impinging on the surface [37–40], $\alpha = 0$ is recovered.

(3) When $\sigma = -3$, an $\alpha = 1/2$ is recovered. Ali and Dey argued that such a scaling law in $E_{tke}(k)$ may be associated with a quasi-two-dimensional (2D) turbulence occurring over a smooth surface (i.e., small N) experiencing an inverse cascade in energy (or forward cascade in enstrophy). While not explicitly discussed by Ali and Dey, it has been shown elsewhere that the energy spectrum due to the presence of the enstrophy cascade leads to a new prediction for the so-called friction factor $f \propto (u_*/U_c)^2$ in rough pipes. This scaling law is $f \sim N^{+1}$ at very high Reynolds number [41]. Naturally, such a friction factor prediction results in $F_{dc} \sim N^{-1/2}$. For three-dimensional (3D) turbulence at very high Reynolds number, $f \sim N^{1/3}$ (Strickler scaling), again consistent with $\alpha = -1/6$.

To recap, the analysis by Ali and Dey makes use of two assumptions: (1) a scaling argument between bulk and local flow variables just above the sediment bed that is independent of the roughness elements [e.g., A_e in Eq. (4)] and (2) a turbulent vertical velocity transporting momentum to the bed with its energy linked to its size by the turbulent kinetic energy spectrum $E_{tke}(k) \propto k^{\sigma}$. Last, to recover the $\alpha = 1/2$, the flow above the surface covered with sediments was assumed to be 2D with an inverse cascade. It is to be pointed out that turbulent flows even above smooth walls are inherently 3D and are dominated by a forward energy cascade thereby prompting interest in alternative explanations to the reported F_{dc}-N scaling relations, especially at small N. The CSB model is now used to explore such an alternative.

B. The cospectral budget model

Accepting the experimental results in Fig. 3, we ask whether a single equation can be derived that recovers the entire F_{dc}-N relations across all N assuming a constant θ_c and a generic shape for the energy spectrum. To answer this question, a phenomenological approach is to be followed that is based on the CSB model. The CSB model has been used to describe flow statistics in wide-ranging applications in stratified atmospheric flows, pipe flow, and open channel flows [34,37,42–47]. In the CSB model, the turbulent shear stress within the roughness sublayer above the bed is linked to the cospectrum using

$$\tau_t = \tau_b = -\rho_f \overline{u'w'} = -\rho_f \int_0^\infty F_{uw}(k)\, dk, \tag{8}$$

where τ_t is the turbulent shear stress or the momentum flux, u' and w' are the turbulent velocity fluctuations in longitudinal (along x) and vertical (along z) directions, respectively, the overline indicates averaging over coordinates of statistical homogeneity, and $F_{uw}(k)$ is the cospectrum. The CSB model must be formulated in the roughness sublayer at some $z = r$ shown in Fig. 1 and is given by

$$\frac{\partial F_{uw}(k)}{\partial t} = P_{uw}(k) + T_{uw}(k) + \pi(k) - D_{uw}(k), \tag{9}$$

with

$$P_{uw}(k) = \Gamma(z) E_{ww}(k); \quad D_{uw}(k) = 2\nu k^2 F_{uw}(k), \tag{10}$$

where r is the thickness of the roughness sublayer assumed to be proportional to d, $P_{uw}(k)$ is a production term responsible for generating correlations between u' and w' at wave number k due to the presence of a finite mean velocity gradient $\Gamma(z) = du/dz$ at height $z = r$ where the CSB model is being formulated, $E_{ww}(k)$ is the vertical velocity energy spectrum at $z = r$, $T_{uw}(k)$ is the

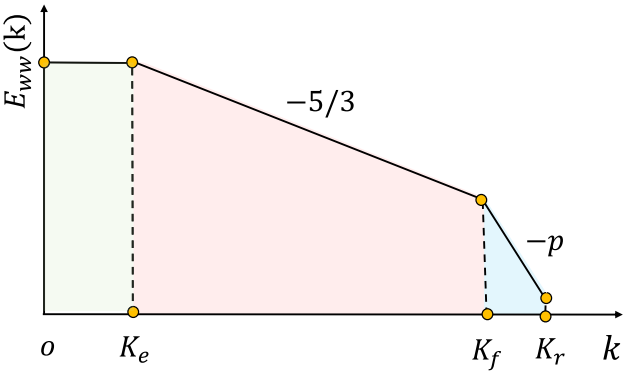

FIG. 4. Schematic of the vertical velocity energy spectrum $E_{ww}(k)$ as a function of wave number k in double-log representation. The right-tail effect is represented with a generic power-law exponent p. K_e, K_f, and K_r are characteristic wave numbers delineating different energy production and transfer regimes in the vertical velocity. To solve the CSB model without depth integration, K_e, K_f, and K_r must be linked to boundary conditions on the flow (i.e., h and d).

momentum flux transfer term across scales, $\pi(k)$ is a pressure-velocity decorrelation term often modeled using return to isotropy principles thereby reducing the correlation strength between u' and w' at scale k, and $D_{uw}(k)$ is a viscous destruction term also responsible for decorrelating w' from u'. The $D_{uw}(k)$ is significant only at scales where the action of fluid viscosity is appreciable, which is determined by the Kolmogorov microscale $\eta = (\nu^3/\epsilon)^{1/4}$, where ϵ is the mean turbulent kinetic energy dissipation rate at $z = r$. Adopting the Rotta closure model for the return-to-isotropy but modified to include the isotropization of the production term [34,42,43,47] yields

$$\pi(k) = -C_R \frac{1}{t_r(k)} F_{uw}(k) - C_I \Gamma(z) E_{ww}(k), \tag{11}$$

where $C_R \approx 1.8$, $C_I = 3/5$ are the Rotta and isotropization of production constants [48,49], and $t_r(k)$ is a wave number-dependent relaxation timescale reflecting the time it takes for local isotropy to be attained for eddies of size $1/k$. When ignoring $D_{uw}(k)$ with respect to $\pi(k)$ for steady-state conditions at high Reynolds number, this CSB model reduces to $P_{uw}(k) = \pi(k)$ allowing the determination of the cospectrum at k:

$$F_{uw}(k) = \frac{1 - C_I}{C_R} \Gamma(z) E_{ww}(k) t_r(k), \tag{12}$$

where a plausible model for $t_r(k) = [k^3 E_{ww}(k)]^{-1/2}$ [50,51] is used. This $t_r(k)$ model recovers $\epsilon^{-1/3} k^{-2/3}$ in the so-called inertial subrange when $E_{ww}(k) \propto k^{-5/3}$. The cospectrum can be integrated across all turbulent scales k to yield the shear stress acting on the bed given by

$$u_*^2 = \frac{\tau_t}{\rho_f} = \frac{1 - C_I}{C_R} \Gamma(z) \int_0^\infty \frac{[E_{ww}(k)]^{1/2}}{k^{3/2}} \, dk. \tag{13}$$

To evaluate the turbulent stress, only the $E_{ww}(k)$ shape above the roughness elements within the roughness sublayer is now required. A schematic of $E_{ww}(k)$ consistent in shape with laboratory and field studies [52–54] is employed and summarized in Fig. 4. Figure 4 presents the main regimes governing the shape of $E_{ww}(k)$: (1) A flat portion presumably due to the randomizing effects of the boundary on the large eddies, (2) an inertial subrange regime characterized by a "$-5/3$" scaling, and (3) a wall-damping regime labeled for convenience as the "p scale." In prior studies where the CSB model was formulated far from a boundary, a simplified flat to $-5/3$ spectrum appeared sufficient at a given height z [37,43,44]. However, for the large-roughness case where the CSB model

is formulated in the roughness sublayer with respect to bulk variables, the tail effects or p scale become significant and offer a link to d. This tail effect has been reported in both field and laboratory experiments [53,55,56] near porous boundaries, where a slope ($p > 5/3$) has been observed above forests and gravel beds alike and even within rod canopies [56]. The aforementioned spectral regimes describing $E_{ww}(k)$ are associated with the following sizes: The flat portion applies to scales larger than $c_1 h(=1/K_e)$, where $c_1 = 0.8$ is adopted based on pipe-flow experiments discussed elsewhere [43], the inertial scaling or $-5/3$ applies to a range of scales bounded by $[K_e, K_f]$, where $K_f < K_r$, $c_2 r(=1/K_r)$, and r is, as before, the thickness of the roughness sublayer assumed to be proportional to d with a proportionality constant of order unity. Many laboratory and field experiments on the roughness height [57,58] show that the value of $c_2 \in [2, 5]$. Here an intermediate value of $c_2 = 3.5$ is employed. The p scaling applies in the range of eddy sizes bounded by $[K_f, K_r]$. Since there is no clear formula available to specify K_f, an *ad hoc* geometric averaging between h and r is adopted, i.e., $K_f = 1/(c_3 h^a r^{1-a})$ where a and c_3 are proportionality coefficients to be determined. Geometric averaging has been proposed for the atmospheric boundary layer when the need arises to determine an intermediate length scale bounded by very large and very small values impacting the flow [54]. For the inertial subrange spectrum, $E_{kol}(k) = C_k \epsilon^{2/3} k^{-5/3}$ is assumed, where $C_k = (24/55)C_k^1$ is the Kolmogorov constant for the vertical velocity and $C_k^1 = 1.5$ [49]. Energy is cascaded from the energy containing range to inertial subrange and is finally released as heat in the dissipation region not explicitly modeled here as the d is assumed to be larger than the Kolmogorov microscale. The $E_{ww}(k)$ drops off rapidly in the viscous dissipation regime so that the overall distortions to the turbulent stress is rather minor when ignored as discussed elsewhere [34]. This assumption is valid only when expressing the CSB model sufficiently high above the roughness elements while maintaining a high Reynolds number so that $r/\eta \gg 1$, where η is, as before, the Kolmogorov length scale. In the regime where eddies are commensurate in size to r, the continuity of $E_{ww}(k)$ across scales requires that the p regime varies as $E_p(k) = C_p \epsilon^{2/3} K_e^{p-5/3} k^{-p}$, where C_p is a proportionality coefficient dependent on p determined as $C_p = c_7 C_k c_3^{5/3-p} c_1^{p-5/3}$. Here c_7 is a similarity coefficient that is connected to p as discussed elsewhere [56]. For an arbitrary p, there is no clear theoretical basis to determine *a priori* c_7. Hence, to constrain the resulting equation and minimize the degrees of freedom in the derivation here, one set of data from Lischtvan and Lebediev was selected and used to compute an optimal $c_7(=8)$. This c_7 value is used for the remaining data sets and sensitivity analyses on p. Moreover, this regime is expected to be significant when the roughness size r is large or the flow is shallow implying the magnitude of K_r is close to K_e. To summarize, the $E_{ww}(k)$ proposed here is allowed to vary with both h and d and experience multiple scaling exponents for differing k. This marks a point of departure from the $E_{tke}(k)$ in Eq. (4) assumed in the derivation of Ali and Dey.

With these eddy-size limits and their connections to the boundary conditions on the flow (h and d),

$$u_*^2 = \frac{\tau_t}{\rho_f} = \frac{1 - C_I}{C_R} \Gamma(z) \int_{K_e}^{K_r} E_{ww}^{1/2}(k) k^{-\frac{3}{2}} \, dk. \tag{14}$$

Adopting the spectral shape in Fig. 4 for $E_{ww}(k)$ results in

$$u_*^2 = \zeta \left[C_p^{1/2} K_e^{\frac{3p-5}{6}} \int_{K_f}^{K_r} k^{-\frac{p+3}{2}} \, dk + C_k^{1/2} \int_{K_e}^{K_f} k^{-7/3} \, dk \right],$$
$$\zeta = \frac{1 - C_I}{C_R} \Gamma(z) \epsilon(z)^{1/3}. \tag{15}$$

In principle, Eq. (15) requires a depth integration to arrive at an expression linking U to u_*. As discussed in Bonetti *et al.* [34], analytical tractability becomes difficult, and only a numerical solution is possible. However, an intermediate approach may be taken if ζ, which is defined by local variables (Γ, ϵ) at $z = r$, can be related to bulk variables (U, h) using naive scaling arguments.

Such intermediate approach bypasses the need for numerical integration and maintains the desired tractability here. It was argued by Gioia and Bombardelli [35] that at $z = r$,

$$\Gamma = \frac{du}{dz} = c_4 \frac{U}{r}; \quad \epsilon = \frac{(c_5 U)^3}{h}. \tag{16}$$

These relations are hereafter labeled as GB02, and they have been used in Ref. [3] when connecting the α in Fig. 3 to σ through the dimensionless $E_{tke}(k)$. Both c_4 and c_5 were originally assumed constants independent of r in GB02, which cannot be realistic. To illustrate why, consider two pipes with identical diameters carrying the same flow rates (or U) but different surface roughness: one pipe is smooth while the other is fully rough. A scaling of the form $\epsilon = (c_5 U)^3/D$ would yield the same bulk or local ϵ for these two pipes unless c_5 includes the roughness effects. To account for such effects, it was assumed elsewhere [34] that the product $c_4 c_5 = c_6 (r/h)^\beta$. When $\beta = 0$, the arguments by GB02 can be recovered, and this limit may be expected for the range covered by the Strickler scaling ($N > 0.01$). We set β to be unity and $c_6 = 0.01$ for $N < 0.01$ and gradually transition to $\beta = 0$ as $N > 0.01$ guided by numerical results from the CSB model reported elsewhere [34] for rough surfaces where the "virtual Nikuradse" equation holds. However, a separate sensitivity to the choice of β is also presented. Inserting these amended GB02 arguments into the CSB model for $\beta = 1$, Eq. (14) can be simplified to

$$\frac{\tau_t}{\rho_f U^2} = D_1 - D_2 N^{\frac{4}{3}(1-a)} + D_3 N^{\frac{p+1}{2}(1-a)} - D_4 N^{\frac{p+1}{2}}, \tag{17}$$

where D_i are coefficients given as

$$D_1 = \frac{3(1-C_I)C_k^{1/2}}{4C_R} c_6 c_1^{4/3}; \quad D_2 = \frac{3(1-C_I)C_k^{1/2}}{4C_R} c_6 c_3^{4/3}$$
$$D_3 = \frac{2(1-C_I)}{C_R} \frac{C_p^{1/2}}{p+1} c_6 c_1^{\frac{5-3p}{6}} c_3^{\frac{p+1}{2}}; \quad D_4 = \frac{2(1-C_I)}{C_R} \frac{C_p^{1/2}}{p+1} c_6 c_1^{\frac{5-3p}{6}} c_2^{\frac{p+1}{2}}. \tag{18}$$

The c_3 is a coefficient determined by a and r/h, and C_p is determined by the p scale regime, and D_1 and D_4 are determined according to empirical coefficients in prior discussion. Hence, only two degrees of freedom (a and c_3) are required to estimate D_2 and D_3 for a preset p. At the critical state when the sediment particles are entrained and upon assuming $r \approx d$, Eqs. (2) and (17) can now be combined to yield a single curve given as

$$\frac{1}{F_{dc}^2} = D_{c1} - D_{c2} N^{\frac{4}{3}(1-a)} + D_{c3} N^{\frac{p+1}{2}(1-a)} - D_{c4} N^{\frac{p+1}{2}}, \tag{19}$$

where $D_{ci} = D_i/\theta_c$ are coefficients involving the Shields number and are assumed to be constant ($\theta_c = 0.06$) at high Re_* as shown in Fig. 2. This is the sought result as it shows how the regimes in the F_c-N are directly linked to the assumed shape of the vertical velocity spectrum. The links between the vertical velocity spectrum and the bulk flow variables are explicitly derived from GB02 subject to some amendments to include roughness effects.

III. RESULTS

For comparison, different values for p are set including the $p = 3$ employed in Ref. [12]. Also, intermediate values (larger than the $-5/3$ scaling) of $p = 2, 7/3$, and $8/3$ are also shown to illustrate the dependence of α on p. For each p value, the CSB model is fitted to the measurements using nonlinear regression, and the agreement is shown in Fig. 5. The corresponding coefficients arising from the data fitting (for each p) are listed in Table I.

Figure 5 suggests that the CSB model can describe the reported measurements in Ref. [3] reasonably. When $p = 3$, which is the value associated with the inverse cascade (or wakes generated by von Kármán streets as discussed elsewhere [59]), a "rebound" zone is identified for $N \in [0.1, 1]$.

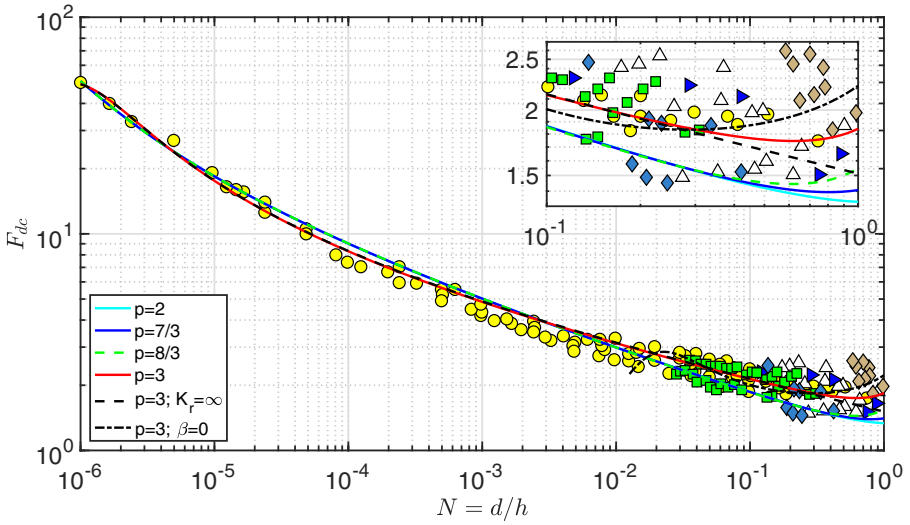

FIG. 5. Fitting the F_{dc}-N derived from the CSB model to the data in Fig. 3. The inset is an enlarged frame associated with the large-roughness regime ($N > 0.1$).

Similarly, when $p > 5/3$, similar rebounds are also predicted by the CSB model. In fact, any value (e.g., $5/3$ to 3) for p will generate a rebound in this zone. This rebound implies that when k is close to K_r, any deviations from the classic $5/3$ scaling in the vertical velocity spectrum influences the link between N and densimetric Froude number. However, the shape of the F_{dc}-N curve for $N \in [10^{-6}, 0.1]$ appears insensitive to the precise choice of p. For this reason, a sensitivity analysis is conducted by reporting the Pearson linear correlation coefficients for a, c_3, C_p, and p as shown in Fig. 6. The Pearson coefficient measures the strength of linear association between two variables and is bounded between -1 and $+1$. The analysis shows that the fitted coefficient a is sensitive to the choice of p as expected, since the Pearson correlation between a and p is close to 1. The magnitude of the correlation between c_3 and p is also large according to Fig. 6. This finding implies that the length scale $1/K_f$ is closely related to the choice of p scale, which is expected. As p increases, the spectrum decays faster indicating the p scale influences the amount of energy in the vertical velocity spectrum above $1/K_f$. The formulation here suggests that the area under the spectrum governed by the $-5/3$ inertial scaling shrinks with K_f shifting closer to K_e and a becomes larger.

Table I shows that K_e contributes more to the intermediate wave number K_f than K_r since a is larger than $(1 - a)$. The analysis here identifies D_{c3} to be the dominant term, which suggests that the tail effects cannot be entirely neglected when linking F_{dc} to N. However, F_{dc} in the range of $N \in [10^{-6}, 0.1]$ appears robust to p variations when all terms are considered. Moreover, when K_r

TABLE I. Values of the relevant coefficients obtained by fitting the CSB model to the F_{dc}-N data in Fig. 3 assuming $c_1 = 0.8$, $c_2 = 3.5$, $c_6 = 0.01$, and $c_7 = 8$.

β	p	D_{c1}	$1 - a$	c_3	C_p	D_{c2}	D_{c3}	D_{c4}
1	2	0.02	0.21	18.81	0.68	1.35	2.07	0.17
1	7/3	0.02	0.20	10.06	0.96	0.59	1.32	0.23
1	8/3	0.02	0.19	6.76	1.45	0.34	1.08	0.32
1	3	0.02	0.11	8.58	0.22	0.47	0.90	0.15
1	3	0.02	0.11	8.53	0.22	0.47	0.89	None
0	3	0.02	0.37	7.60	0.25	0.40	0.74	0.15

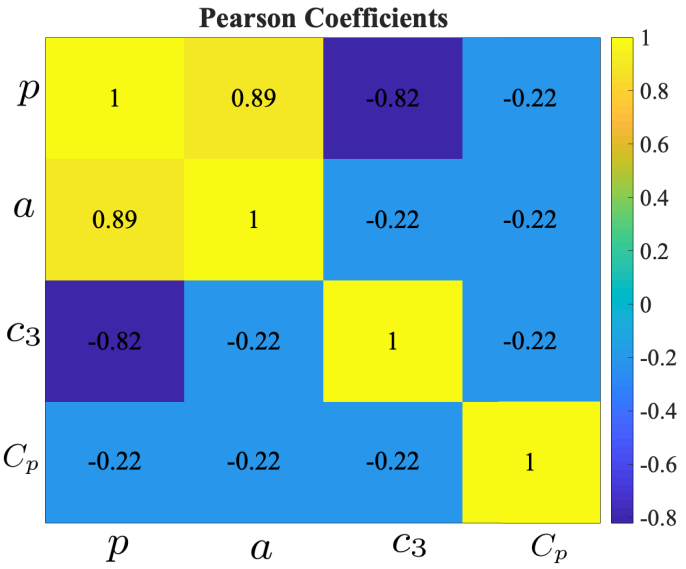

FIG. 6. Pearson correlation coefficients among a, c_3 and C_p corresponding to a given p. For example, the Pearson coefficient of two random variables (X, Y) is calculated as the covariance, $\mathrm{cov}(X, Y)$ normalized by the standard deviations of the individual variables $(=\sigma_X, \sigma_Y)$, i.e., $\mathrm{cov}(X, Y)/(\sigma_X \sigma_Y)$. Strong correlations are shown between p and a and between p and c_3.

is extended to $+\infty$, which is shown in the black dashed line, the rebound is no longer observed. This finding indicates that the spectral distortion in the vicinity of 5/3-law play an important role in large-scale roughness (i.e., $N > 0.1$), but not across all N values. According to GB02, β approaches zero for $N \in [10^{-2}, 1]$ to be consistent with the Stickler scaling for this range of N. If such scaling is adopted and $\beta = 0$ in Eq. (19) throughout, then

$$\frac{1}{F_{dc}^2} = D_{c1} N^{-1} - D_{c2} N^{\frac{1}{3}(1-4a)} + D_{c3} N^{\frac{p}{2}(1-a)-\frac{1}{2}(1+a)} - D_{c4} N^{\frac{p-1}{2}}. \tag{20}$$

By setting $p = 3$, the modeled result from Eq. (20) is also shown in Fig. 5. For $N \in [10^{-2}, 1]$, Eq. (20) also captures the data reported in Ref. [3] where a rebound does not appear. However, for $N \in [10^{-6}, 10^{-2}]$, Eq. (20) fails to reproduce the entire F_{dc}-N relation, which confirms that GB02 scaling arguments cannot be applied in the range $N \in [10^{-6}, 10^{-2}]$ without modifications.

IV. CAUTIONARY COMMENTS AND MODEL LIMITATIONS

The CSB model proposed here by no means offers finality to explaining the F_{dc}-N diagram reported by Ali and Dey [3], and its limitations are briefly reviewed. Before delving into the model limitations, a number of cautionary comments are warranted about the processes being represented by the data in Ref. [3]. To begin with, the connection between U_c and sediment incipient motion across many experiments may not be as universal as implied by Fig. 3. For example, other data sources and studies [60] contradict the entire concept of critical velocity used in Ref. [3]. A number of laboratory measurements also suggest that no unique threshold velocity appears to be linked to sediment movement [61]. The Reynolds number range over which θ_c is experimentally independent of Re_* must be viewed with caution. In flume experiments with water ($\nu = 1 \times 10^{-6}$ m^2 s^{-1}), $u_* = (ghS_o)^{1/2}$, typical $h = 1$ m and $S_o = 0.01$ lead to an estimate of $u_* = 0.3$ ms^{-1} as a typical friction velocity. To maintain $\mathrm{Re}_* > 400$ requires a minimum $d = 400\nu/u_* \approx 1 \times 10^{-3}$ m. Hence, a minimum $N = d/h = 1 \times 10^{-3}$ can be experimentally maintained without θ_c being dependent

on Re_*. This estimate is orders of magnitude larger than the $N \in [10^{-6}, 10^{-4}]$ reported in Ref. [3] describing the scaling relation $F_{dc} \propto N^{-1/2}$. The finding here implies that the F_{dc}-N scaling at the finest $N \in [10^{-6}, 10^{-4}]$ cannot be experimentally accessed for a θ_c strictly independent of Re_* using water (or air) as fluids in typical flumes (or wind tunnels). A θ_c that varies linearly with Re_*^{-1} (expected for $\mathrm{Re}_* \ll 1$) may lead to an adjustment of the F_{dc}-N relation by a factor that scales as $d^{-3/4}N^{1/4}$ in both the Ali and Dey and the CSB analysis. For $\mathrm{Re}_* \in [3, 400]$, the situation may be subtler. The θ_c varies from a minimum of 0.02 to a maximum of 0.06, but the variations in $(\theta_c)^{1/2}$ are between 0.14 and 0.24, which is much smaller than the factor of 10 variations in F_{dc} for $N \in [10^{-6}, 10^{-4}]$. So pragmatically, a near constant $(\theta_c)^{1/2}$ may still be acceptable even in the range of $N \in [10^{-6}, 10^{-4}]$, perhaps explaining the robustness of the $\alpha = 1/2$ for this range of N in typical flume experiments.

From a theoretical perspective, the space-time distribution of eddies on and within the bed is needed, and formal double averaging must be used to obtain up-scaled approximations starting from single-particle equations and its interaction with neighboring particles. The CSB model proposed here makes no such attempt and it must be viewed only as a complementary explanation to the insightful but piecewise analysis offered by Ali and Dey [3]. The CSB model accounted for only two terms: a stress production and pressure decorrelation. Transfer of stresses across scales as well as molecular effects are ignored (though they can be incorporated in principle). Moreover, the CSB model assumed that the time for the return to isotropy at any scale can be inferred from the vertical velocity energy content, which may not be a valid approximation (relaxation time and time to isotropy can differ for differing k regimes). Perhaps among the most *ad hoc* assumptions made in the CSB model derivation are links between local and bulk variables. While the links employed here accommodate expected deviations from those proposed by GB02 and used in Ref. [3], they remain questionable across the entire range of roughness values. Another *ad hoc* assumption is the links between the transition zones across scales in the assumed vertical velocity spectrum and the variables h and d. To assess how robust the findings here are to these assumed links, a sensitivity analysis was conducted. This analysis identified the zones where assumptions about the p scale impacted the entire F_{dc}-N curve.

Despite all the aforementioned criticisms, it is safe to state that the work here provides a single expression that summarizes the data featured by Ali and Dey [3]. The theoretical argument leading to this single expression may be viewed as naive but pragmatic. Thus, the expression derived here may be imminently used in models aimed at describing sediment transport across large spatial domains, a topic that is gaining prominence given the advancement in remote sensing platforms.

V. CONCLUSION

The multiscaling regimes of sediment entrainment encoded in the F_{dc}-N curve reported by Ali and Dey [3] have been considered using a cospectral budget model where integration across all turbulent scales and z are needed. A single expression that links F_{dc} to N was proposed using the CSB model that recovers all six decades of N variations. The CSB model shows that the vertical velocity spectrum $E_{ww}(k)$ can explain the entire F_{dc}-N curve, not just piecewise scaling. Moreover, the k^{-3} scaling used by Ali and Dey, a signature of an enstrophy cascade dominating the spectrum, is not necessary *per se*. The CSB model highlights another issue rarely considered when linking spectral exponents to scaling laws in the F_{dc}-N curve: Inferring local variables from bulk variables. This inference is by no means straightforward, especially for N values that fall outside the original Strickler N regime. Studies using the so-called virtual Nikuradse [34,62] as well as studies dealing with intermittency corrections to turbulent spectra [63,64] all point to deviations from the Strickler scaling for $N \in [10^{-6}, 10^{-2.5}]$. These effects were partly accommodated for through a nonzero β here.

While the CSB model can describe quantitatively the measured F_{dc}-N curve, its three key parameters a, c_3, and C_p cannot be predicted on theoretical grounds. To be able to predict these

coefficients requires models that describe the shape of the vertical velocity spectrum (including any transition zones) only as a function of d, h, and U, a topic that is better kept for future research.

ACKNOWLEDGMENTS

The authors thank A. Packman for the many constructive comments and helpful suggestions on an earlier version of this manuscript. G.K. acknowledges support from the US National Science Foundation (NSF-AGS-1644382 and NSF-IOS-1754893).

[1] C. T. Yang, Incipient motion and sediment transport, J. Hydraul. Div. **99**, 1679 (1973).
[2] P. Y. Julien, *Erosion and Sedimentation* (Cambridge University Press, New York, 2010), pp. 112–126.
[3] S. Ali and S. Dey, Origin of the scaling laws of sediment transport, Proc. R. Soc. A **473**, 20160785 (2017).
[4] G. K. Gilbert and E. C. Murphy, The transportation of debris by running water. No. 86. US Government Printing Office, 1914.
[5] M. C. Miller, I. N. McCave, and P. D. Komar, Threshold of sediment motion under unidirectional currents, Sedimentology **24**, 507 (1977).
[6] Z. Jiang and P. K. Haff, Multiparticle simulation methods applied to the micromechanics of bed load transport, Water Resour. Res. **29**, 399 (1993).
[7] A. G. Hunt, A probabilistic treatment of fluvial entrainment of cohesionless particles, J. Geophys. Res.: Solid Earth **104**, 15409 (1999).
[8] I. McEwan, M. Sørensen, J. Heald, S. Tait, G. Cunningham, D. Goring, and B. Willetts, Probabilistic modeling of bed-load composition, J. Hydraul. Eng. **130**, 129 (2004).
[9] A. Shields, Anwendung der aehnlichkeitsmechanik und der turbulenzforschung auf die geschiebebewegung, Ph.D. thesis, Technical University Berlin, 1936.
[10] A. B. Shvidchenko, G. Pender, and T. B. Hoey, Critical shear stress for incipient motion of sand/gravel streambeds, Water Resour. Res. **37**, 2273 (2001).
[11] Z. Cao, G. Pender, and J. Meng, Explicit formulation of the Shields diagram for incipient motion of sediment, J. Hydraul. Eng. **132**, 1097 (2006).
[12] S. Dey and S. Ali, Advances in modeling of bed particle entrainment sheared by turbulent flow, Phys. Fluids **30**, 061301 (2018).
[13] J. M. Buffington and D. R. Montgomery, A systematic analysis of eight decades of incipient motion studies, with special reference to gravel-bedded rivers, Water Resour. Res. **33**, 1993 (1997).
[14] M. H. García, E. M. Laursen, C. Michel, and J. M. Buffington, The legend of AF Shields, J. Hydraul. Eng. **126**, 718 (2000).
[15] S. Dey and A. Papanicolaou, Sediment threshold under stream flow: A state-of-the-art review, KSCE J. Civil Eng. **12**, 45 (2008).
[16] P. R. Wilcock, Critical shear stress of natural sediments, J. Hydraul. Eng. **119**, 491 (1993).
[17] A. E. Lobkovsky, B. Jensen, A. Kudrolli, and D. H. Rothman, Threshold phenomena in erosion driven by subsurface flow, J. Geophys. Res.: Earth Surf. **109**, F04010 (2004).
[18] M. Church and M. A. Hassan, Mobility of bed material in Harris Creek, Water Resour. Res. **38**, 1 (2002).
[19] M. Righetti and C. Lucarelli, May the Shields theory be extended to cohesive and adhesive benthic sediments? J. Geophys. Res.: Oceans **112**, C05039 (2007).
[20] G. Parker, P. R. Wilcock, C. Paola, W. E. Dietrich, and J. Pitlick, Physical basis for quasi-universal relations describing bankfull hydraulic geometry of single-thread gravel bed rivers, J. Geophys. Res.: Earth Surf. **112**, F04005 (2007).
[21] C. Parker, N. J. Clifford, and C. R. Thorne, Understanding the influence of slope on the threshold of coarse grain motion: Revisiting critical stream power, Geomorphology **126**, 51 (2011).

[22] P. L. Wiberg and J. D. Smith, Calculations of the critical shear stress for motion of uniform and heterogeneous sediments, Water Resour. Res. **23**, 1471 (1987).
[23] P. D. Komar, Comparisons of the hydraulics of water flows in Martian outflow channels with flows of similar scale on Earth, Icarus **37**, 156 (1979).
[24] J. F. Kok, An improved parametrization of wind-blown sand flux on Mars that includes the effect of hysteresis, Geophys. Res. Lett. **37**, L12202 (2010).
[25] D. M. Burr, J. P. Emery, R. D. Lorenz, G. C. Collins, and P. A. Carling, Sediment transport by liquid surficial flow: Application to Titan, Icarus **181**, 235 (2006).
[26] S. Ali and S. Dey, Impact of phenomenological theory of turbulence on pragmatic approach to fluvial hydraulics, Phys. Fluids **30**, 045105 (2018).
[27] L. L. Lischtvan and V. V. Lebediev, Gidrologia i gidraulika v mostovom doroshnom, straitielvie, in *Hydrology and Hydraulics in Bridge and Road Building* (Gidrometeoizdat, Leningrad, USSR, 1959).
[28] C. R. Neill, Mean-velocity criterion for scour of coarse uniform bed-material, in *Proceedings of the 12th Congress of International Association for Hydraulic Research, Fort Collins, Colorado, USA* (1967), Vol. 3, pp. 46–54 .
[29] K. Ashida and M. Bayazit, Initiation of motion and roughness of flows in steep channels, in *Proceeding of the 15th Congress of International Association for Hydraulic Research, Istanbul, Turkey* (1973), Vol. 1, pp. 475–484.
[30] M. L. Olivero, Movimiento incipiente de partículas en flujo torrencial, Special Report: University of Los Andes, Meridad, Venezuela, 169 (1984).
[31] J. Aguirre-Pe and R. Fuentes, Movement of big particles in steep, macro-rough streams, in *Proceeding of the 24th Congress of International Association for Hydraulic Research, Madrid, Spain* (1991), Vol. A, pp. 149–158.
[32] J. C. Bathurst, W. H. Graf, and H. H. Cao, Initiation of sediment transport in steep channels with coarse bed material, in *Mechanics of Sediment Transport*, edited by B. M. Summer and A. Muller (1982), pp. 207–213.
[33] J. C. Bathurst, H. H. Cao, and W. H. Graf, The data from the EPFL study of hydraulics and sediment transport in a steep flume, Report No. CH-1015, Ecole Polytechnique Fédérale de Lausanne (EPFL), Lausanne, Switzerland 64 (1984).
[34] S. Bonetti, G. Manoli, C. Manes, A. Porporato, and G. Katul, Manning's formula and Strickler's scaling explained by a co-spectral budget model, J. Fluid Mech. **812**, 1189 (2017).
[35] G. Gioia and F. A. Bombardelli, Scaling and Similarity in Rough Channel Flows, Phys. Rev. Lett. **88**, 014501 (2001).
[36] G. Gioia, N. Guttenberg, N. Goldenfeld, and P. Chakraborty, Spectral Theory of the Turbulent Mean-Velocity Profile, Phys. Rev. Lett. **105**, 184501 (2010).
[37] T. Banerjee and G. Katul, Logarithmic scaling in the longitudinal velocity variance explained by a spectral budget, Phys. Fluids **25**, 125106 (2013).
[38] P. Drobinski, P. Carlotti, J. L. Redelsperger, V. Masson, R. M. Banta, and R. K. Newsom, Numerical and experimental investigation of the neutral atmospheric surface layer, J. Atmos. Sci. **64**, 137 (2007).
[39] G. Katul and C. R. Chu, A theoretical and experimental investigation of energy-containing scales in the dynamic sublayer of boundary-layer flows, Boundary-Layer Meteorol. **86**, 279 (1998).
[40] G. Katul, A. Porporato, and V. Nikora, Existence of k^{-1} power-law scaling in the equilibrium regions of wall-bounded turbulence explained by Heisenberg's eddy viscosity, Phys. Rev. E **86**, 066311 (2012).
[41] N. Guttenberg and N. Goldenfeld, Friction factor of two-dimensional rough-boundary turbulent soap film flows, Phys. Rev. E **79**, 065306(R) (2009).
[42] G. Katul, A. Porporato, C. Manes, and C. Meneveau, Co-spectrum and mean velocity in turbulent boundary layers, Phys. Fluids **25**, 091702 (2013).
[43] G. Katul and C. Manes, Cospectral budget of turbulence explains the bulk properties of smooth pipe flow, Phys. Rev. E **90**, 063008 (2014).
[44] G. Katul, A. Porporato, S. Shah, and E. Bou-Zeid, Two phenomenological constants explain similarity laws in stably stratified turbulence, Phys. Rev. E **89**, 023007 (2014).

[45] G. Katul, D. Li, H. Liu, and S. Assouline, Deviations from unity of the ratio of the turbulent Schmidt to Prandtl numbers in stratified atmospheric flows over water surfaces, Phys. Rev. Fluids **1**, 034401 (2016).
[46] D. Li, G. Katul, and S. Zilitinkevich, Closure schemes for stably stratified atmospheric flows without turbulence cutoff, J. Atmos. Sci. **73**, 4817 (2016).
[47] K. A. McColl, G. Katul, P. Gentine, and D. Entekhabi, Mean-velocity profile of smooth channel flow explained by a cospectral budget model with wall-blockage, Phys. Fluids **28**, 035107 (2016).
[48] B. E. Launder, G. Reece, and W. Rodi, Progress in the development of a Reynolds-stress turbulence closure, J. Fluid Mech. **68**, 537 (1975).
[49] S. B. Pope, *Turbulent Flows* (Cambridge University Press, Cambridge, 2000), p. 754.
[50] G. K. Vallis, *Atmospheric and Oceanic Fluid Dynamics* (Cambridge University Press, Cambridge, 2017), p. 936.
[51] D. Li and G. Katul, On the linkage between the $k^{-5/3}$ spectral and $k^{-7/3}$ cospectral scaling in high-Reynolds number turbulent boundary layers, Phys. Fluids **29**, 065108 (2017).
[52] G. J. Kunkel and I. Marusic, Study of the near-wall-turbulent region of the high-Reynolds-number boundary layer using an atmospheric flow, J. Fluid Mech. **548**, 375 (2006).
[53] C. Manes, D. Poggi, and L. Ridolfi, Turbulent boundary layers over permeable walls: Scaling and near-wall structure, J. Fluid Mech. **687**, 141 (2011).
[54] K. G. McNaughton, R. J. Clement, and J. B. Moncrieff, Scaling properties of velocity and temperature spectra above the surface friction layer in a convective atmospheric boundary layer, Nonlinear Proc. Geophys. **14**, 257 (2007).
[55] D. Cava and G. Katul, Spectral short-circuiting and wake production within the canopy trunk space of an alpine hardwood forest, Boundary-Layer Meteorol. **126**, 415 (2008).
[56] D. Poggi and G. Katul, Two-dimensional scalar spectra in the deeper layers of a dense and uniform model canopy, Boundary-Layer Meteorol. **121**, 267 (2006).
[57] R. D. Hey, Flow resistance in gravel-bed rivers, J. Hydraul. Div. **105**, 365 (1979).
[58] L. C. Van Rijn, Sediment transport, Part III: bed forms and alluvial roughness, J. Hydraul. Eng. **110**, 1733 (1984).
[59] D. Poggi, G. Katul, and B. Vidakovic, The role of wake production on the scaling laws of scalar concentration fluctuation spectra inside dense canopies, Boundary-Layer Meteorol. **139**, 83 (2011).
[60] J. W. Lavelle and H. O. Mofjeld, Do critical stresses for incipient motion and erosion really exist? J. Hydraul. Eng. **113**, 370 (1987).
[61] T. Pähtz and O. Durán, The cessation threshold of nonsuspended sediment transport across aeolian and fluvial environments, J. Geophys. Res.: Earth Surf. **123**, 1638 (2018).
[62] B. H. Yang and D. D. Joseph, Virtual Nikuradse, J. Turbulence **10**, N11 (2009).
[63] N. Goldenfeld and G. Gioia, Roughness-Induced Criticality in Turbulence, Phys. Rev. Lett. **96**, 044503 (2006).
[64] M. Mehrafarin and N. Pourtolami, Intermittency and rough-pipe turbulence, Phys. Rev. E **77**, 055304(R) (2008).